

# Gold prospectivity mapping through generation and integration of geophysical, geochemical, remote sensing, and geological evidence layers in Saqez area, NW Iran

Farzaneh Mami khalifani <sup>a, \*</sup>, Samaneh Barak <sup>b</sup>, Maysam Abedi <sup>b</sup>, Saeed Yousefi <sup>c</sup>

<sup>a</sup> Department of Earth Science, University of New Brunswick, Canada.

<sup>b</sup> School of Mining Engineering, College of Engineering, University of Tehran, Iran.

<sup>c</sup> Faculty of Engineering, University of Birjand, Iran.

## Article History:

Received: 01 May 2023.

Revised: 15 June 2023.

Accepted: 17 June 2023.

## ABSTRACT

This study serves to demonstrate the application of geophysical data interpretation in order to recognize the structural features related to the mineralization. The aforementioned structures generate the evidence layers, which undergo augmentation and enhancement processes. This results in the production of evidence layers that, when integrated with other geo-exploration evidence layers, contribute to the delineation of mineral exploration targets with increased reliability. In this study, the utilization of aeromagnetic and radiometric data is illustrated for the recognition of structural features and host rocks associated with orogenic gold mineral systems. Furthermore, the integration of geophysical data interpretation, specifically the identification of mineralization-related features, with alterations and the geochemical signature of mineralization is demonstrated. This integration facilitates the delimitation of exploration targets with improved dependability.

**Keywords:** *Orogenic gold deposit; Airborne geophysics; Geological data; Saqez property; Mineral prospectivity mapping.*

## 1. Introduction

Orogenic gold deposits are distinguished as the main and the most typical Gold in the world. [37, 8, 60, 36, 79]. This type of deposit is formed as a result of the structural setting occurring in orogenic belts. The distribution of gold deposits is significantly influenced by geological lineaments. Major faults, which are primary faults, along with secondary faults and shear zones (minor faults), as well as folds, play a crucial role in regulating the movement of fluids [36, 32, 15]. Such structural features may provide permeable pathways facilitating transportation of hydrothermal fluids containing minerals from sources to deposition sites [25, 24, 15]. Consequently, the analysis of spatial relationship between faults and crustal fractures could lead us forward to mineralized zones [22].

The geometric characteristics of fault systems observed in gold deposits provide evidence that the majority of these structures are not located at shallow depths. Consequently, the utilization of additional exploration techniques, such as geophysics, becomes necessary to identify and evaluate deeper-seated structures [27]. Aeromagnetic survey has been employed as a well-known and reliable geophysics data to investigate and seek such hidden structures related to gold deposits [15, 53]. The identification of the boundaries of intrusive bodies and lineaments through magnetic intensity analysis has been widely acknowledged as advantageous in the field of mineral exploration. It is noteworthy to mention that the radiometric survey, which is a commonly employed geophysical tool, can also be utilized to simultaneously gather data on the main host rocks of gold deposits, alongside airborne magnetic data [43, 28, 66].

This study aims (i) to examine airborne magnetic and radiometric data in order to extract and identify geological features associated with

gold mineralization. (e.g., structures and host rocks) and (ii) to utilize the identified features along with other indications of mineralization obtained from the processing of geochemical and remote sensing data. This combined information will be used to define the zones that are most favorable for the occurrence of gold mineralization in the Saqez district.

## 2. Geological setting, structure and mineralization

The study area under investigation is situated in the northern region of the Sanandaj-Sirjan Zone (SSZ) in northwest Iran, spanning longitudinally from E 46°00' 00" to 46°30' 00" and latitudinally from N 36°00' 00" to 36°30' 00". The SSZ extends over a distance of 2000 km, starting from the east Anatolian fault in Turkey and extending to the Oman fault. It is bounded by the Zagros orogenic belt to the southwest and the Urumieh-Dokhtar magmatic belt to the northwest (Fig. 1a). The Sanandaj-Sirjan Zone (SSZ), as well as prominent tectonic regions such as the Zagros thrust fold belt and Urumieh-Dokhtar magmatic arc, has its genesis in the subduction process of the Neo-Tethys Ocean floor beneath the Iran-Turkey region. Subsequently, this subduction resulted in the collision between the subducted slab and the Arabian plate, culminating in the formation of the Zagros Orogeny during the Late Cretaceous epoch [68, 40].

The SSZ constitutes mostly Mesozoic units with relatively rare Precambrian-Paleozoic rocks that generally occur in the southeastern part of the zone. The pronounced deformation and metamorphism of these geological units were induced by the Zagros Orogeny. Additionally, these units exhibit a consistent NW-SE alignment, which

\* Corresponding author: E-mail address: farzaneh.mamikhalfani@unb.ca (F. Mami khalifani).

corresponds to the prevailing pattern observed in the adjacent structures of the Zagros fold-thrust belt to the southwest and the Urumieh-Dokhtar zone to the northeast. The entire stratigraphic sequence is characterized by the presence of numerous intrusive bodies, both deformed and undeformed in nature [34].

Paleozoic units were formed in a stable continental platform to epicontinental shelf and subsequently overlaid by volcano-sedimentary rocks during the Permo-Triassic opening of the NeoTethy Ocean. This rifting phase was related to basalt, diabase and some intermediate volcanic rocks and calcareous succession overlying unconformably older rocks. Late Paleozoic-Middle Mesozoic sequences are mainly shallow water calcareous to volcano-sedimentary rocks associated ultrabasic intrusive bodies [65]. Silicic to intermediate magmatic activity related to deposition of volcano-sediments occurred in the SSZ during Middle-Late Mesozoic. Throughout Cenozoic time, deposition of marine bioclastic carbonate and saline anhydrite beds, deltaic-river channel sand and clastic rocks which have relation with intrusive rocks suggests a widespread regression and establishing a stable condition [34].

Presence of rare Cenozoic formations and widespread Mesozoic-Paleozoic rock units with respecting to deformed and non-deformed intrusive bodies and volcanic sequences divulges a complex metamorphic and deformation tectonic history for the SSZ. This zone was in a stable continental setting by late Paleozoic when this role shifted to calc-alkaline magmatic arc during the Mesozoic time.

The tectonic history of the Zone reveals the occurrence of two distinct regional accretion deformation events: one during the Late Jurassic-Early Cretaceous period and the other during the Late Cretaceous period. [9]. These events were assigned to initiation of subduction and the convergent deformation that is associated with the process of crustal thickening, respectively. Earlier investigations have demonstrated the exhibition of various deformation styles and tectonic vergences in SSZ which can be attributed to prominent deep-seated structures oriented in a northwest direction [34]. The late Mesozoic convergent deformation across the SSZ resulted in SW-trending vergent, NW-SE abundant tight to isoclinal folded structures and thrust faulting leading to uplifting of deep metamorphic rocks. During Mesozoic time, these tectonic and metamorphic events resulted in the recognition of a NW-trending orogenic belt and development of gold deposits along it [35, 14].

Based on the type of gold deposits, the SSZ has been divided into three metallogenic subzones: the northern, central, and southern SSZ. This subzone is mainly covered by 100 k Saqez geological map published by Geological Survey of Iran that contains the location of several orogenic gold deposits [13]. These gold deposits exhibit similar characteristics to other deposits found in the vicinity of major fault systems along the Sanandaj-Sirjan Zone (SSZ), as illustrated in Figure 1c. The Saqez subzone represents a metamorphic belt controlled by NE-trending faults, which hosts several well-known orogenic gold deposits including Qabaqloujeh, Kervian, Kasnazan, Hamzeh-Gharanein, and Qolqoleh. The Saqez geological map (Fig 1b) reveals that the oldest country rocks in the area consist of highly deformed metamorphic and magmatic rocks from the Precambrian era, encompassing schist, amphibole gneiss, felsic volcanic rocks, and the Doran granite. Paleozoic consequences are mainly carbonates and sandstones followed by Mesozoic mafic, metavolcanic, and metavolcano-sedimentary rocks associated with mylonized granitic bodies. The geological formations of the region encompass Cenozoic limestone, mafic to intermediate volcanic rocks, and occasional granitic intrusions [14]. A prominent deep thrust fault governs the spatial distribution of ancient metamorphic rocks, intrusions, and gold deposits within the Saqez subzone. This observation implies a connection between deep-seated faults, magmatic events, and gold mineralization in the northern segment of the Sanandaj-Sirjan Zone (SSZ). The existence of two significant faults, one oriented NW-SE and the other NE-SW, appears to have played a pivotal role in controlling the genesis of established gold deposits in the area [13]. Through a combination of geochemical and structural analysis, Aliyari et al. (2012) identified two distinct types of mineralization and structural styles, namely ductile and brittle

deformation. The presence of brittle/ductile shear zones, where deformation is localized, likely influenced rock permeability, thereby regulating fluid movement and mineralization within the Saqez subzone. These intrusions may have also acted as efficient thermal drivers for fluid circulation. Figure 1c illustrates the density map of faults and a rose diagram, derived from field surveys, demonstrating a close correlation between the sources of gold and orogenic activities within the southwestern portion of the Saqez prospect zone.

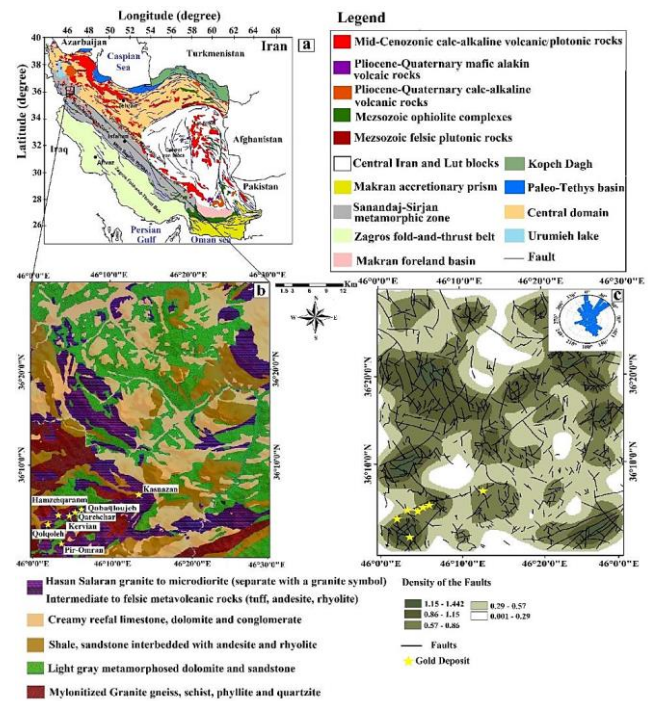


**Fig. 1.** (a) The Saqez prospecting zone in Iran is depicted in its geographical location, (b) the geological map with 1:100000 scale, and (c) the faults, density and rose diagram of all extracted faults from geology map.

### 3. Methods and results

In this study, the geo-scientific datasets were compiled by integrating diverse evidential layers obtained from multiple sources, including the geological map at a scale of 1:100,000, ASTER images, airborne magnetic and radiometric data, and multi-element geochemical data. These datasets encompassed the Saqez prospect zone. Subsequently, all collected data underwent a processing phase to ensure compatibility and enhance their analytical potential. In 1976, the collection of airborne geophysical data was conducted by the Atomic Energy Organization of Iran. The flight lines were positioned around 500 meters apart, maintaining an altitude of 120 meters. In the subsequent subsections, initial processing of magnetometry and radiometric data was conducted to identify concealed shallow and deep-seated geological lineaments that likely exert control over multi-system orogenic and intrusion-related gold-bearing mineralization. Subsequently, different bands of ASTER imagery were utilized to identify areas exhibiting alteration patterns and prominent lineaments. Additionally, geological field operations were employed to discern primary faulted regions. Finally, stream sediment geochemical data were statistically analyzed to separate anomalous Au zones from non-anomalous background regions using the C-N multifractal approach [61, 38, 45, 29]. A general workflow shown in Fig.2 was followed to investigate exploratory evidential layers in order to construct geo-science datasets.

#### 3.1. Aeromagnetic data

Geophysical data, specifically airborne magnetometry, offers valuable insights into both surface and subsurface geological lineaments as well

as magmatic sources associated with intrusions. To identify the boundaries of magmatic intrusions, which are often linked to mineralization, numerous image processing methods have been developed. These techniques are designed to detect prominent geophysical magnetic anomalies resulting from the presence of intrusions [26, 27]. These techniques could enhance the trace of shallow or deep-seated geological features by suppressing or amplifying magnetic signals. Edges of the magnetic anomalies are matched with the boundaries of various rock units differentiated by their magnetic susceptibility properties. Therefore, the lineaments of the faults and shear zones can be derived from such anomalies. These features are permeable environments for transferring and circulating the Au-bearing fluids to the upper level of the earth crust. In addition, identification of the ultramafic igneous units associated to the gold mineralization is another significant key of mineralization that can be detected from various filters developed for processing magnetometry data [62, 33]. The Geosoft Oasis Montaj software was employed in this study to improve the quality of the airborne geophysical data.

Directional derivatives of the potential field geophysics data are basis of various advantageous filters for calculating the gradient of the magnetic field intensity, where they act as a high pass filter to suppress the long magnetic wavelength of the deep-seated sources [10, 64, 55]. To strengthen the magnetic amplitude arising from shallow sources, the first vertical derivative of potential field data (magnetic and gravity) gives rise to a gradient map, in which the trace of the near surface sources is drastically enhanced. As a result, one of the important applications of such filter is to extract and enhance the traces of magnetic lineaments arising from geological contacts and the boundary of the rock units [18].

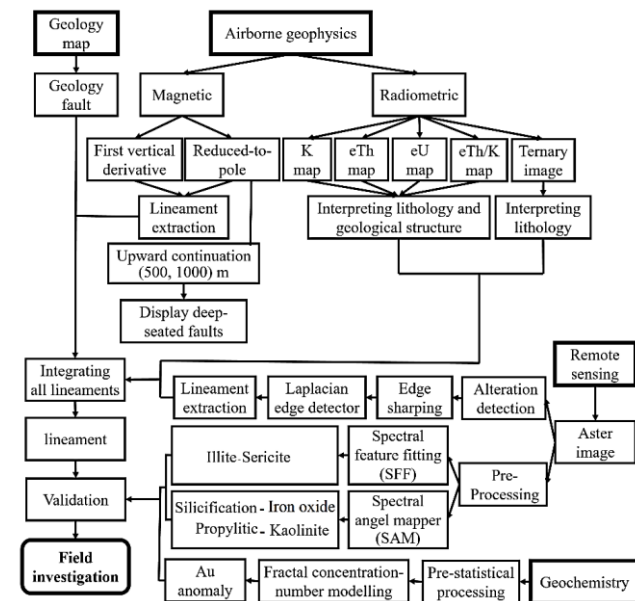


**Fig. 2.** The workflow is followed to localize favorable zones responsible for gold mineralization.

The inclination and declination angles of the Earth's magnetic field in the Saqez area were measured to be a number of 53.7 and 3.5 degrees, respectively. To enhance the delineation of the Au-bearing mineralization sources, likely associated with magmatic intrusion units, as well as the detection of geological lineaments, the regional magnetic influence was mitigated by employing an optimal polynomial surface. This surface was utilized to estimate and eliminate the regional or background magnetic field across the entire study area, resulting in a surface characterized by a zero-degree magnitude. In fact, the data acquired exhibited a strong resemblance to the IGRF model, accurately representing the Earth's magnetic field. Subsequently, the magnetic data underwent calculations using the reduced-to-pole (RTP) technique,

resulting in an enhanced magnetic signal.

As an initial filtering step, the RTP technique was utilized to convert the original data into magnetic pole coordinates. This transformation helps to diminish the influence of the Earth's magnetic field inclination and aligns the positive segment of the magnetic signal with the primary source of the anomaly [63]. A symmetric pattern of the RTP outputs can facilitate the interpretation of the magnetic anomalies, where the positive pole shows the location of causative target [6, 21]. Figure 3 displays the RTP (Reduced-To-Pole) map covering the Saqez prospect zone, which facilitated the visual extraction of structural characteristics. Notably, the areas of heightened RTP values exhibited a clear spatial correspondence with the presence of intrusive magmatic units, as depicted in the geological map (Fig. 1). Specifically, these units were identified as granite formations situated in the southern and eastern sectors of the Saqez zone. Among these intrusive masses, the Hasan Salaran granite, known to have served as the conduit for silica fluids responsible for governing the gold mineralization process, was identified. To extract magnetic lineaments, simultaneous consideration of the RTP and its vertical magnetic gradient were taken into account to reveal the major/minor structural features (i.e., large and small length faults) along with the location of intrusive magmatic masses responsible for the targeted mineralization [37]. According to the obtained geological lineaments and rose diagram plot, the general trend of these structures was mostly along the NE-SW and NW-SE directions. These directions were perpendicular and parallel to the SSZ, respectively. The gold deposits in the southwestern part of the region are situated along the path of the identified faults, specifically the NE-SW lineaments.

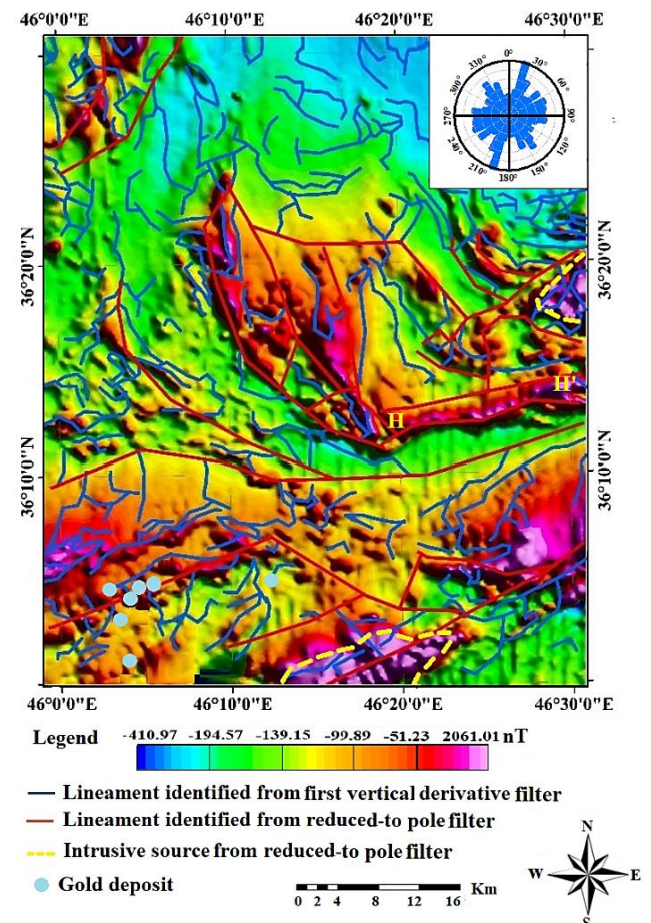


**Fig. 3.** The extracted lineaments were obtained by analyzing the magnetic data, including the RTP map and its vertical gradient. These lineaments were then overlaid with a rose diagram to visualize their distribution.

The upward continuation method is another usable filter in which long wavelengths are detected, mostly arising from deeper magnetic sources [16, 49]. Indeed, it minimizes the effects of shallow sources and environmental noises by attenuating high frequency (short wavelength) magnetic signals. This filter continues the potential field observations to an altitude further away from the causative sources with a stable mathematical process in Fourier domain, leading to enhancing deep magmatic intrusions [5, 18]. In this study, the process of upward continuation was conducted using various altitudes, employing a trial-and-error approach. Specifically, the upward continuation was performed at two distinct altitudes, namely 500 m and 1000 m, for the RTP data. The resulting continuation outcomes at these altitudes are illustrated in Figure 4. The trace of major faults (HH') along with the location of the intrusive magmatic units Leucogranite (G3) (blue line) were manifested. Both maps effectively demonstrated the vertical expansion of these features, indicating their depth extension. The presence of these augmented tectonic structures played a pivotal role in facilitating the accumulation of substantial volumes of hydrothermal fluids and their circulation within geological lineaments.

### 3.2. Airborne radiometric data

The data acquired through airborne radiometric surveys can serve as a valuable exploratory dataset for several purposes. Firstly, it can be utilized to identify hydrothermally altered regions that exhibit spatial proximity to gold deposits. Secondly, it can aid in the identification and localization of magmatic intrusive units and felsic igneous rocks, which are known to possess a notable abundance of radioactive elements such as potassium (K), uranium (U), and thorium (Th). Lastly, the dataset can be utilized to delineate geological lineaments, which serve as primary controlling factors in the mineralization process. [67, 4, 15, 28, 1].

The main secondary group of host rocks in the study region comprises of mylonitic granites and their altered counterparts. These rocks have higher concentrations of radioactive elements, including feldspar, plagioclase, and zircon, within their compositions [15]. Drawing from previous investigations involving geochemical and stable isotope analyses, the genesis of gold deposits within the Saqez region is believed to be linked to a series of geological processes. These processes include deep-seated metamorphic devolatilization, dehydration reactions, and the liberation of gold from metamorphic and metavolcanic rock formations. It is postulated that the granitoid rocks present in the area served as a source of heat for the mobilization of

gold-bearing fluids. Furthermore, in conjunction with the radiometric survey, the aeromagnetic data provided insights into the presence of minerals such as magnetite, titanomagnetite, and ilmenite within mafic and metavolcanic rocks across the study area. [15].

Fig. 5 depicts the radiometric maps representing Potassium (K), equivalent Thorium (eTh), equivalent Uranium (eU), and the ratio of K/eTh. The pink and red areas in the K enrichment map (Fig. 5a) were associated to the hydrothermal alteration from felsic rocks such as granites and granite-gneiss (Mtgr-gn) (white boundary), granite and granite-gneiss of Tamoteh mass (G1) (black boundary), Hassan Salaran granite mass (G2) (cream boundary), and Leucogranite (G3) (blue boundary), where these rocks were the main hosts of the orogenic gold deposits in the Saqez area. The utilization of a Potassium (K) enrichment map played a crucial role in identifying areas characterized by potassic alteration, which serves as a valuable indicator for the occurrence of gold mineralization. The geological context surrounding the study area consisted of diorite and gabbro masses, represented by the color green. Conversely, regions depicted in blue corresponded to the presence of carbonatite rocks, including limestone, slaty shale, and schist stone units within the Jurassic clastic sequences, shale, sandstone, and microconglomerate. These blue regions exhibited lower concentrations of potassium content (Fig. 5a). The eTh map showed similar spatial pattern similar to the K map, where the borders of the host rocks of the gold mineralization were superimposed on the map shown in Fig. 5b.

The highest levels of the uranium concentration depicted with pink colors in Fig. 5c were associated to the gneiss and granite-gneiss (Mtgr-gn), whereas the Hassan Salaran granite represented a moderate level of the eU (cream boundary). In addition, shale and sandstone rocks corresponded to the lowest values of the eU. The K/eTh ratio map, as depicted in Figure 5d, demonstrated a significant correlation with the spatial distribution of hydrothermal alteration patterns and the pathways of fluid flow. This correlation aligned closely with the occurrence and distribution of granites and granite-gneiss rocks within the study area [11, 15].

A widely recognized method for visualizing airborne radiometer data involves the utilization of a ternary color scale, whereby the maps of K/eTh/eU are assigned distinct red, green, and blue (RGB) colors, respectively [28, 54]. In the resulting ternary map, felsic igneous units such as gneiss, granite-gneiss (Mtgr-gn), and the granite masses G1, G2, and G3 exhibited comparatively elevated concentrations of radioactive elements. Consequently, these areas appeared as white in the ternary map visualization (Fig. 6).

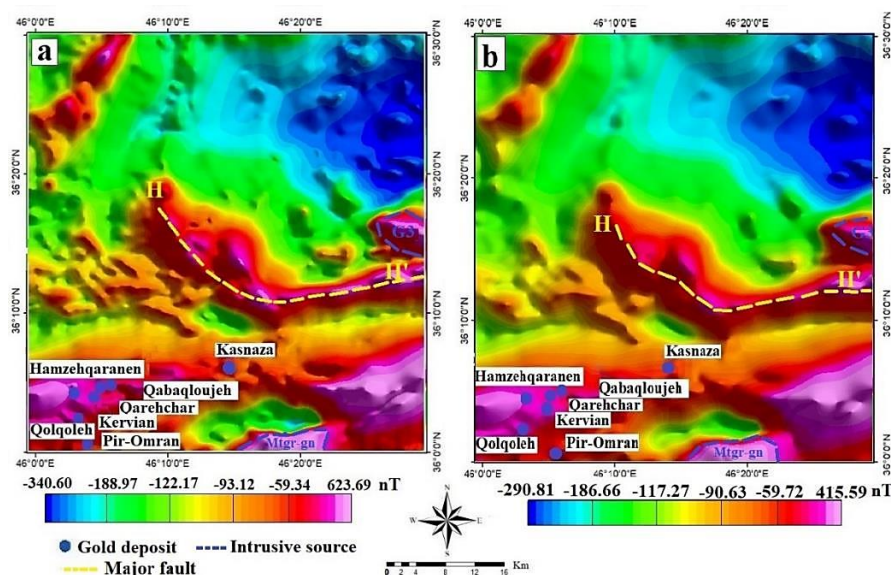
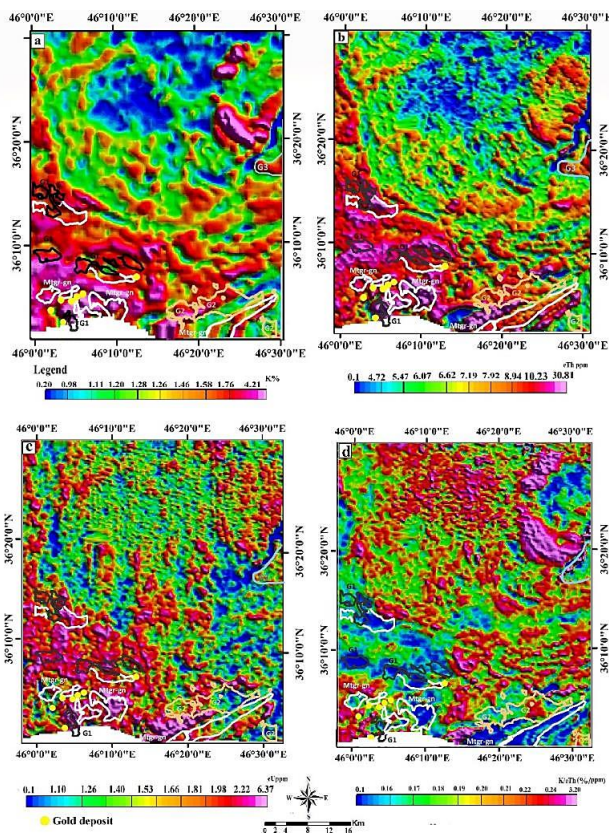


Fig. 4. (a) The RTP magnetic data was extended vertically to two different altitudes, namely 500 m, and (b) 1000 m. Additionally, the maps display the location of certain gold deposits overlaid on them.



**Fig. 5.** (a) The concentration maps include Potassium (K) concentration map, (b) equivalent Thorium (eTh) concentration map, (c) equivalent Uranium (eU) concentration map, and (d) Potassium/Thorium (K/eTh) ratio map. The boundaries marked in black, white, blue, and cream represent different rock masses, namely granite and granite-gneiss of Tamoteh mass (G1), gneiss and granite-gneiss (Mtgr-gn), Leucogranite (G3), and Hassan Salاران granite mass (G2), respectively.

These rock units were aligned with the main faults HH' in the prospect region (drawn in Figs. 3, 4 and 6) as well. Dark colors areas represented mafic igneous units containing very few amounts of the radioactive elements in contrary to the felsic units with the white color. The white regions observed in the southern part of the area, near the Qolqoleh, Kervian, and Qabagloujeh deposits, encompassed both altered and unaltered granite-mylonite units. These granite-mylonite units, exhibiting a white-pinkish color, could potentially serve as hosts for gold mineralization. Furthermore, in the eastern section of the area along the yellow line (HH'), pinkish-red colors were identified, which can be attributed to potassium enrichment within intruded masses along the fault, coinciding with the Saqez fault. By considering the outcomes of the airborne geophysical surveys (magnetometry and radiometric data), the eastern and southwestern regions of the prospect area, characterized by granite, granite-gneiss, and leucogranite formations, emerged as favorable zones for hosting gold-bearing mineralization.

### 3.3. Satellite imagery data

In this study, ASTER (Advanced Spaceborne Thermal Emission and Reflection Radiometer) imagery data was utilized, with a pixel size of 30 meters. The imagery data had a minimal cloud cover of approximately 0%. The dataset was acquired through a sophisticated multispectral satellite equipped with three distinct subsystems designed to capture imagery across different wavelength ranges. These subsystems included the visible near-infrared (VNIR) range, covering 0.4-1.4  $\mu\text{m}$ , the short-wave infrared (SWIR) range spanning 1.4-2.5  $\mu\text{m}$ , and the thermal-

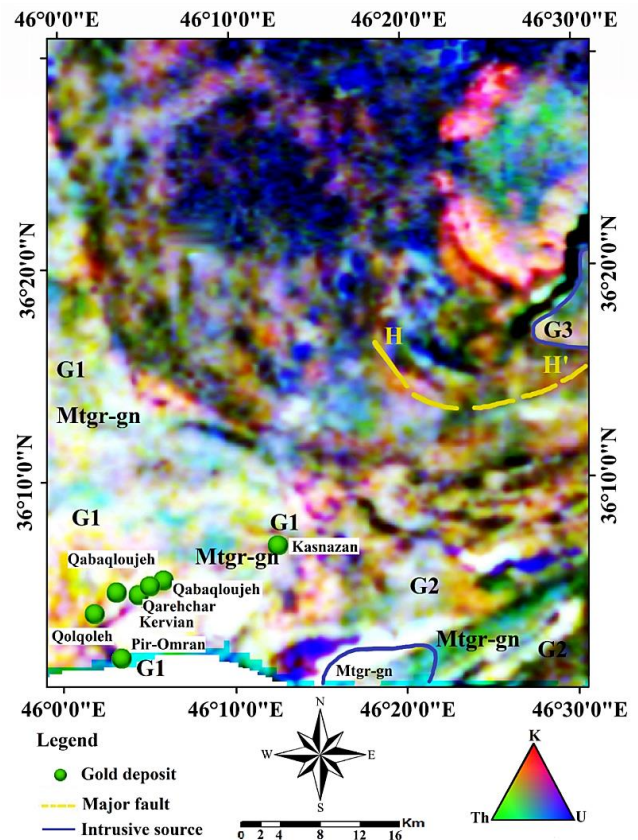


**Fig. 6.** Radiometric ternary color scale map (in 2D) generated from the K/eTh/eU elements.

infrared (TIR) range encompassing 8.0-14.0  $\mu\text{m}$ . The satellite provided data across 14 bands within these regions [50]. Many researchers have acknowledged the broad applicability of ASTER data in mapping hydrothermal alteration and extracting geological lineaments [57, 58, 50, 2, 22, 3]. The process of alteration mapping holds significant importance in the initial stages of most exploration programs. In this regard, the utilization of multispectral remote sensing images proves highly valuable as it efficiently contributes to mineral prospectivity mapping, resulting in notable time and cost savings [70, 51].

Before initiating the processing stages of the ASTER images, some pre-processing stages are required to outperform the generated results. By utilizing the Internal Average Relative Reflectance (IAR Reflectance) filter, the ASTER images were normalized based on the spectral average of the scene. A false reflected image was produced to identify mineral absorption features through the log residuals approach. In addition, spectral angle mapper (SAM) as a famous technique in the classification of the satellite imagery data, was applied to evaluate the spectral resemblance for quenching the influence of the shading and accentuating the target reflectance characteristics [42]. Indeed, the calculated angle between spectra is responsible for presenting the grade of similarity between them [71].

The Spectral Angle Mapper (SAM) approach has been recognized as a highly effective method for alteration mapping in comparison to other techniques such as band ratio (BR), principal component analysis (PCA), spectral feature fitting (SFF), false color composite, match filtering, and methods similar to them [80, 81, 69, 46]. The ENVI software (version 4.8) was employed to apply the Spectral Angle Mapper (SAM) method for the purpose of mapping various alterations linked to the orogenic gold mineralization system. These alterations encompass propylitic, kaolinite, iron oxide, and silicification, as illustrated in Fig. 7.

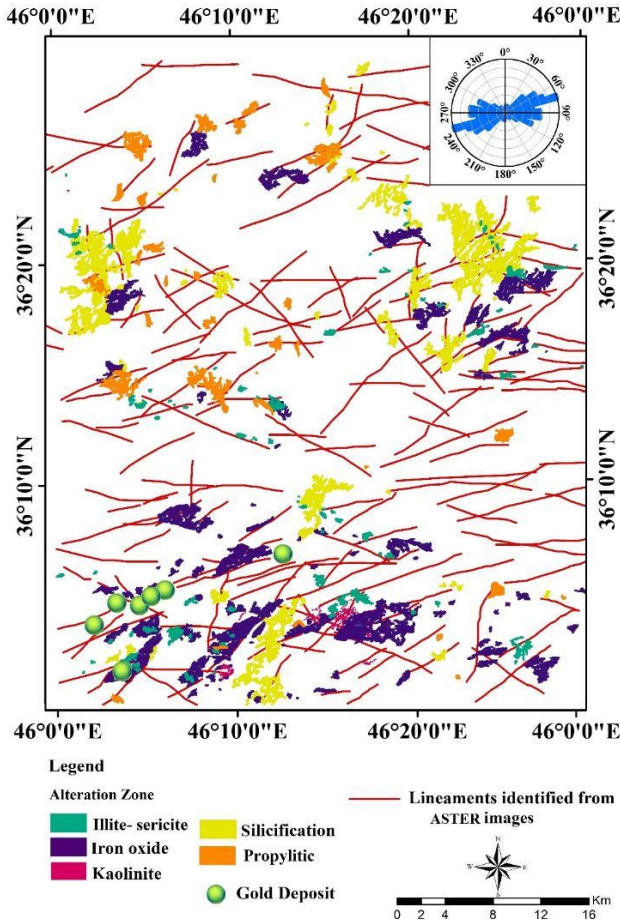


**Fig. 7.** The spatial distribution of alteration zones and extracted faults from the ASTER images in the Sazeq area is presented along with a rose diagram plot.

In this study, the endmember spectra library obtained from the Jet Propulsion Laboratory (JPL1) was utilized. The presence of chlorite was considered as an indicator for the propylitic zone, while kaolinite was indicative of kaolinite alteration. Hematite spectra were used as a reference for iron oxide alteration, and quartz spectra were utilized for detecting silicification alteration [12, 20]. The shadow intensity observed in the images derived from the SAM method was dependent on the level of similarity between the endmember spectra and the spectra associated with each pixel [31, 50]. The optimal angles obtained from the SAM method, which effectively detected alteration zones, are presented in Table 1.

Spectral Feature Fitting (SFF) is an additional methodology utilized in mineral exploration for identifying specific alterations through the matching of spectral libraries. The SFF approach produces three distinct outputs, namely root-mean-square (RMS), scale, and fit images. The root-mean-square (RMS) image quantifies the average difference between the spectrum of the image and the reference spectrum (Jpl1) derived from the library. The scale image is generated for each endmember to align the unknown spectra with the reference library spectra.

**Table 1.** Optimum angles (in radians) derived from the SAM method employed to the ASTER data.

Endmember	Optimum angle (radians)	Color of alteration area in map
Chlorite	0.130	Orange
Kaolinite	0.120	Pink
Hematite	0.180	Purple
Quartz	0.100	Cream

Finally, the fitted image aids in aligning the reference spectrum with the unknown spectrum, facilitating a more accurate comparison [59]. The same endmembers (Jpl1) and 0.5-2.5  $\mu\text{m}$  spectral region were assumed for implementing the SFF technique, similar to those for the SAM, to determine illite-sericite alteration. The sericite was considered as the reference spectra for imaging this alteration [17].

The highest score, which indicates the closest match between sericite and the unknown spectrum, was found to be 0.7 in this particular analysis. In Fig. 7, various alterations associated with orogenic gold-bearing mineralization systems were presented. Notably, iron oxide alteration exhibited the closest spatial correlation with the gold deposits in the southwestern areas of the study region.

Furthermore, in order to identify geological lineaments alongside the alteration mapping conducted using satellite imagery data, a high-pass filter was implemented on the ASTER images using Geomatica software (version 2017-04-03). Various linear and nonlinear spatial high-pass operators, such as Laplacian, Ford, directional filters, Sobel, and Kirsch techniques, have been proposed for this purpose [48]. To eliminate the mountain ridges as uncorrelated features in gold mineralization, a two-step process was employed. Firstly, an edge sharpening filter was applied, followed by the utilization of the Laplacian edge detector. As a result, the correlated lineaments associated with mineralization, such as faults, contacts, and boundaries of intrusive magmatic units, were successfully extracted. To further analyze their distribution, a rose diagram was generated (Fig. 7).

Fig. 8 presents all structural geological features extracted from the exploratory geo-science datasets (geology map, remote sensing, and geophysics). Notably, the plotted ones are simultaneously visible on all maps (Figs. 1c, 3, and 7).

Following their length, the extracted lineaments were categorized into two main groups: major and minor. These lineament groups predominantly displayed a strike direction in the NE-SW and NW-SE orientations.

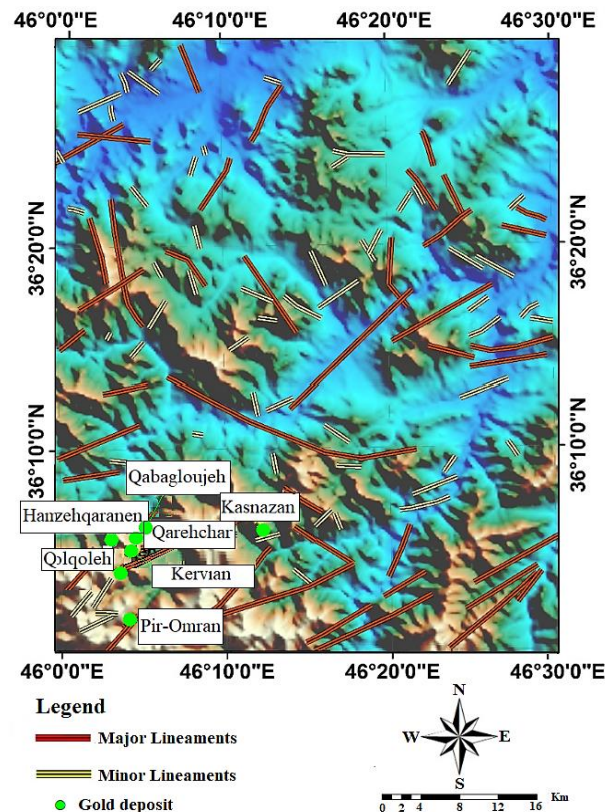


**Fig. 8.** The final structural feature extracted from all exploratory data in the Sazeq region superimposed on the digital elevation model. These features are simultaneously visible on all exploratory maps.

### 3.4. Geochemical data

Geochemical surveys have proven to be an effective exploration tool in identifying anomalies associated with gold mineralization on a district scale [56, 24, 39]. A key aspect of geochemical exploration is the separation of background values from anomalous values [76, 77, 78, 52, 72, 73, 30, 35]. Fractal methods have been utilized to determine thresholds for separating geochemical anomalies [82]. In the study area considered in this paper, a total of 1063 stream sediment samples were collected, and analytical analysis was conducted for 21 elements, including Au, W, Hg, Ba, Mn, Mo, Sn, Co, Sb, As, Cu, Bi, Ni, V, Cr, Ag, Pb, Zn, B, Be, and Ti, using the ICP-MS approach. The geochemical survey comprehensively covered the entire prospect region, as shown in Figure 9. The objective was to differentiate between anomalous and background regions through statistical analysis. These analyses involved addressing censored data, handling outliers, and normalizing the regional stream sediment data. Subsequently, enrichment index (EI) values were calculated for each element.

Table 2 provides a comprehensive overview of the statistical properties associated with the analyzed elements. Figures 10a and 10b depict the histogram and probability plots of the transformed Au concentration values, represented as EI values. These plots clearly indicate a departure from normality in the distribution of the data. Recognizing the impact of non-normality on various statistical techniques, two normalization methods, namely logarithmic and Cox-Box transformations, were employed to address this issue. After evaluating the skewness and level of normality observed in the dataset, the Cox-Box normalization technique was selected and implemented using Minitab software version 17.1.0. This approach facilitated the normalization of the EI data, aligning it more closely with a normal distribution. (Figs. 10c and 10d).

A cluster analysis, as a multivariate statistical processing method, was carried out on the data to investigate the spatial similarity between the Au concentration variation and other elements [19, 47, 41]. The results of the abovementioned analysis are shown in Fig. 11. The analysis revealed a partial similarity between the Au element and two other elements, W and Sb. The C-N multifractal method was employed to the EI values of the Au, Sb and W data (Figs.12a, b, and c), leading to the separation of the probable anomalous regions from the backgrounds.

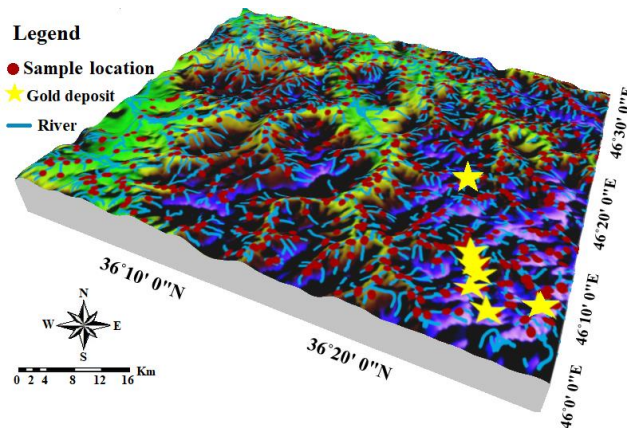


Fig. 9. Location of 1063 stream sediment samples on the DEM map in the Saqez area.

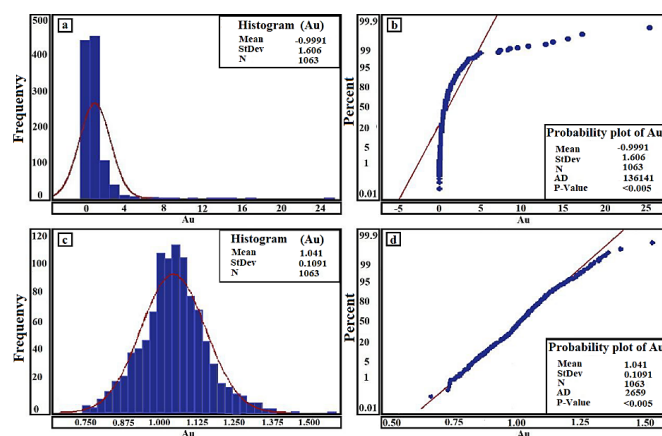
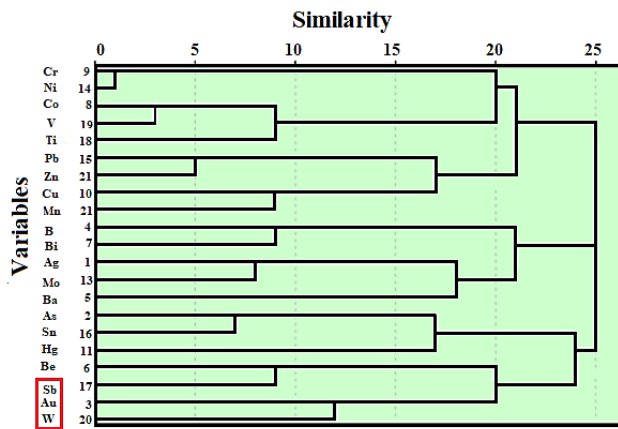


Fig. 10. The histogram and probability plots display the EI values of the Au concentrations, with the upper row representing non-normal data and the lower row representing the normalized values.

Table 2. The statistical properties of the geochemical elements in the Saqez region.

	Range	Min	Max	Average	Std. deviation	Skewness	Kurtosis
Ag (ppm)	0.448	0.028	0.476	0.088	0.033	2.258	151.17
As (ppm)	273.33	0.76	274.1	12.27	26.86	4.29	25.37
Au (ppb)	184.73	0.08	739.26	0.72	23.66	28.83	889.03
B (ppm)	191.9	3.8	195.7	35.4	18.94	1.61	6.45
Ba (ppm)	2892	309	3201	478	200.73	8	78.34
Be (ppm)	4.8	0.9	5.7	1.8	0.52	2.11	10.10
Bi (ppm)	1.55	0.1	1.65	0.19	0.13	3.59	22.64
Co (ppm)	50.1	8.4	58.5	23.2	7.37	0.76	0.85
Cr (ppm)	404.6	46.6	451.2	152.8	51.66	0.72	1.45
Cu (ppm)	191.3	6.4	197.7	30.3	11.72	4.10	43.74
Hg (ppm)	9.94	0.009	9.95	0.037	0.41	15.97	333.53
Mn (ppm)	2486	263	2749	853	267.09	1.31	5.04
Mo (ppm)	8.42	0.29	8.71	0.92	0.64	4.20	30.33
Ni (ppm)	194.5	14.7	209.2	82.1	33.84	0.64	0.34
Pb (ppm)	139.9	8.7	148.6	22.5	9.31	3.62	33.55
Sb (ppm)	159.6	0.4	160	0.92	9.31	11.32	148.51
Sn (ppm)	18.1	0.7	18.8	2.6	1.62	3.23	17.78
Ti (ppm)	9180	1581	10761	3813	1169.52	1.23	2.73
V (ppm)	250.3	43	293.3	130.1	41.49	0.51	0.03
W (ppm)	9.6	2	11.6	2.5	0.90	3.68	19.38
Zn (ppm)	277	37	314	77	24.38	1.78	9.13



**Fig. 11.** The outcome of the cluster analysis was performed on all geochemical elements in the Saqez area.

Considering four threshold values, the distribution maps of Au, Sb, and W concentrations were categorized into five classes representing zones with very low, low, medium, high, and very high favorable potential. Fig. 13 is able to reveal that the SW parts of the Saqez had high potential of the gold mineralization. The favorable region identified exhibits strong alignment with all the processed evidential layers derived from diverse geoscience datasets. These datasets encompass the alteration maps (Fig. 7), extracted lineaments (Fig. 8), magnetometry maps (Figs. 3 and 4), and radiometric maps (Fig. 5 and 6). The substantial consistency observed across these datasets enhances the credibility and importance of the identified favorable region in the study area.

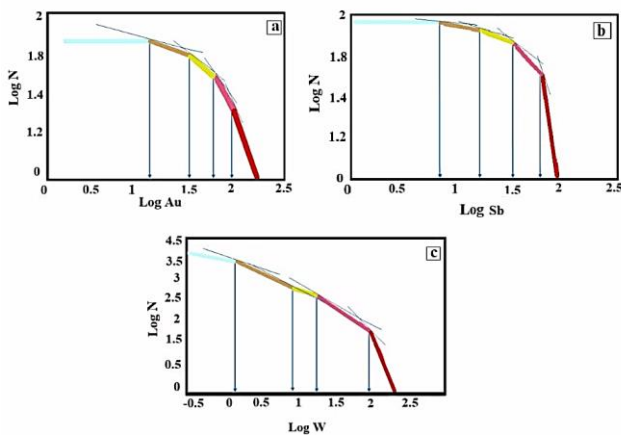


**Fig. 12.** (a) Logarithmic diagram of the C-N multifractal model for Au, (b) for Sb, and (c) for W.

#### 4. Results and Discussion

Gold mineralization within the Saqez zone predominantly occurs within shear zone structures and faults that have undergone compressive deformation, displaying both ductile and brittle characteristics. As a consequence of these geological processes, various rock units such as gneiss, granite-gneiss, and mylonitic granites have undergone alteration. To map these structural features in the area, a multi-scale edge detection method was implemented using aeromagnetic, radiometric, and remote sensing data. The predominant orientation of significant geological lineaments is observed in the NW-SE and NE-SW directions. Several deposits containing gold mineralization, including Hamzehqaranen, Qolqoleh, Qabagloujeh,

Qarehchar, Kervian, Pir-Omran, and Kasnazan, are concentrated in the southwestern region. It is noteworthy that these deposits exhibit a strong association and alignment with the identified geological lineaments, as illustrated in Figs. 14 and 15. The multi-disciplinary geoscience datasets comprising of the airborne geophysics, remote sensing, geochemistry, and geological studies were constructed and overlaid all footprints to delimit the prospect region into some potential areas for future exploration programs. Figure 14 shows a 3D model including the lineaments, alteration, and geochemical anomalies that are related to gold deposits. The identified favorable mineralized zones were found in close proximity to the gneiss, granite-gneiss, mafic to intermediate metavolcanic, sericite schist and mylonitic granite, phyllite, Hasan Salaran granite, and andesite host rocks. In addition, gold mineralization observed in the silica and carbonatite veins as well, gotten enriched in the silicified areas (Fig. 7). Microscopic studies on the Au-bearing rocks (Fig. 14) by Aliyari et al. (2012, 2014) demonstrated that the shear zones have controlled most of the mineralized zones. It is worth mentioning that AA' fault with largest elongation in the region is started from the NW to the east which bends toward HH' fault. The BB' fault at the SW of the Saqez was strongly associated with the known mineralized zones. The HH' (Saqez-Sardasht) fault with a length of about 100 km, parallel to the BB', was also located at the east part of the area, which could have been prospect for the gold mineralization due to its coincidence with the dense fault system and the altered rocks.

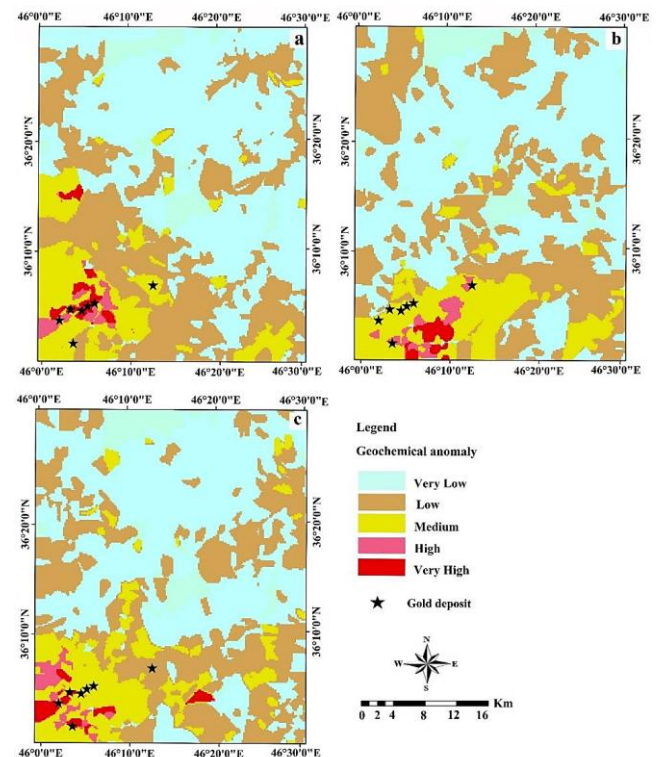


**Fig. 13.** Geochemical anomaly map reclassified using the C-N multifractal model for (a) Au, (b) Sb, and (c) W.

The integration of various geological features, including lineaments, host rock, alteration zones, and anomalous geochemical regions, revealed a strong correlation with the gold deposits located in the southwestern region of the prospecting zone, as illustrated in Figure 15a. These features were also observed in the western and eastern portions, indicating the need for further exploratory studies in these areas. The rose diagram of the extracted geological lineaments, shown in Figure 15b, demonstrated a notable spatial association between the NE-SW faults, which were perpendicular to the shear zone structure (SSZ), and the deposits in the southwestern regions. Figs. 14 and 15a provided a

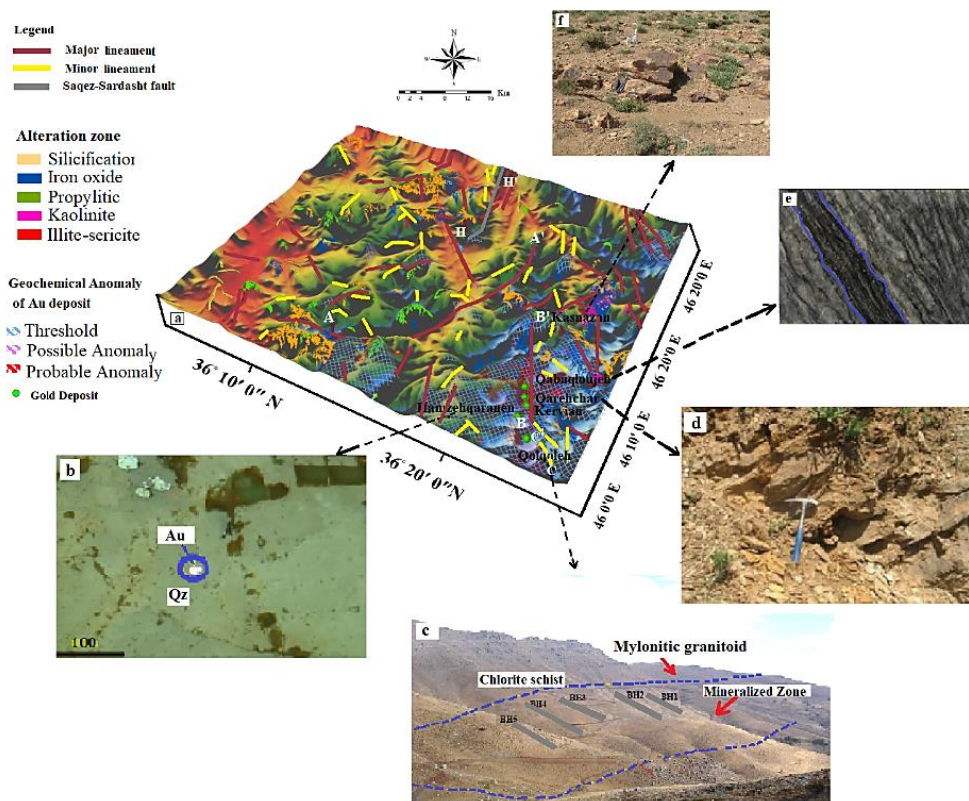


**Fig. 14.** The DEM map illustrated in 3D (a), the Au particles in a quartz background from Hamzehqaranen deposit (b), the faults within shear zones in the Qolqoleh (c), the chlorite-schists in Qarehchar (d), the sulfide Au-bearing ore, blue bands are mostly quartz and feldspar in Qabaqloujeh (e), and the outcrops alterations of silicification and sericite in Kasnazan (f), (Aliyari et al., 2014, Almasi et al. 2017).

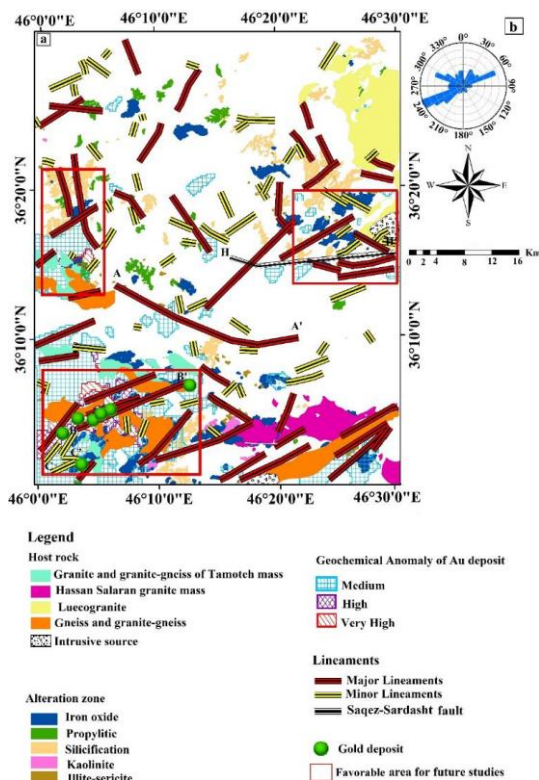


**Fig. 15.** Integrated faults, host rock, intrusive source, alteration zones and anomalous geochemical regions from all exploratory geo-science datasets and the identified favorable areas for further exploration (a) along with their rose diagram plot (b).

comprehensive representation of both major and minor lineaments, exhibiting both NE-SW and NW-SE orientations, alongside the host rocks, intrusive magmatic sources, alteration zones, and anomalous geochemical/geophysical regions. This suggests that the most promising zones for orogenic gold mineralization were predominantly aligned along the NE-SW trending lineaments.

### 5. Conclusions

The identification and characterization of geological lineaments, including faults, shear zones, and geological contacts, as well as the mapping of alterations, geochemical anomalies, and geophysical anomalies, have yielded valuable insights into the orogenic gold mineralization process. These findings contribute significant information to our understanding of the mineralization system in the study region. In this research, the mineral favorability mapping was generated by overlaying various exploration indicators derived from multi-disciplinary geo-science datasets (i.e., airborne geophysics, remote sensing images, geochemical and geological data) in the Saqez prospecting zone, at the west part of Iran. To reduce the uncertainty arising from such prospectivity mapping, different algorithms and datasets were utilized. Additionally, the following conclusions can be noted:

- The results revealed that among the two patterns observed in the fault systems, characterized by trends in the northwest-southeast and northeast-southwest directions, it was the latter that exerted a more significant control on gold mineralization.
- Shear zones facilitated the circulation of the intrusive magmatic fluids especially in the SW of the Saqez prospect, where several deposits have occurred in an orogenic-based system. These zones with fractured tectonic activity were also spatially associated with the anomalous geochemical contents, geophysical anomalies and altered zones.
- In comparison to the mineralization observed in the southwestern

portions, two favorable regions located in the eastern and western areas of the Saqez zone exhibit similar characteristics that indicate their potential for gold mineralization. Therefore, these regions should be given due consideration for future exploration programs.

-This study highlights the significance of incorporating additional structural features and generating augmented evidence layers through the interpretation of geophysical data. By doing so, the delimitation of the study area can be refined, resulting in the identification of more reliable exploration targets.

## Acknowledgments

The authors gratefully appreciate the School of Mining Engineering, University of Tehran, for all support, and the Geological Survey of Iran (GSI) for data preparation.

## REFERENCES

- [1] Abbass, A.A., Fidelis, I.K., & Shakarit, B.A. (2023). Interpreting the magnetic signatures and radiometric indicators within Kogi State, Nigeria for economic resources. *Geosystems and Geoenvironment*, 2(2), p.100157.
- [2] Abdelkareem, M., & El-Baz, F. (2017). Characterizing hydrothermal alteration zones in Hamama area in the central Eastern Desert of Egypt by remotely sensed data. *Geocarto International*. 1-19.
- [3] Abd El-Wahed, M., Kamh, S., Abu Anbar, M., Zoheir, B., Hamdy, M., Abdeldayem, A., Lebda, E.M., & Attia, M. (2023). Multisensor satellite data and field studies for unravelling the structural evolution and gold metallogeny of the Gerf Ophiolitic Nappe, Eastern Desert, Egypt. *Remote Sensing*, 15(8), p.1974.
- [4] Abedi, M., Gholami, A., & Norouzi, G.H. (2013). A stable downward continuation of airborne magnetic data: A case study for mineral prospectivity mapping in Central Iran. *Computer & Geoscience*. 52, 269-280.
- [5] Abedi, M., Gholami, A., & Norouzi, G.H. (2014). A new stable downward continuation of airborne magnetic data based on Wavelet deconvolution. *Near Surface Geophysics*. 12(6), 751-762.
- [6] Abedi, M., & Oskooi, B. (2015). A combined magnetometry and gravity study across Zagros orogeny in Iran. *Tectonophysics*. 664, 164-175.
- [7] Abedi, M., Norouzi, G.H., & Fathianpour, N. (2015). Mineral potential mapping in Central Iran using fuzzy ordered weighted averaging method. *Geophysical Prospecting*. 63(2), 461-477.
- [8] Abedi, M., Kashani, S. B. M., Norouzi, G. H., & Yousefi, M. (2017). A deposit scale mineral prospectivity analysis: A comparison of various knowledge-driven approaches for porphyry copper targeting in Seridune, Iran. *Journal of African Earth Sciences*, 128, 127-146.
- [9] Agard, P., Omrani, J., Jolivet, L., & Mouthereau, F. (2005). Convergence history across Zagros (Iran): constraints from collisional and earlier deformation. *International journal of earth sciences*. 94(3), 401-419.
- [10] Aghajani, H., Moradzadeh, A., & Zeng, H. (2009). Estimation of depth to salt domes from normalized full gradient of gravity anomaly and examples from the USA and Denmark. *Journal of Earth Science*. 20 (6), 1012.
- [11] Airo, M.L. (2007). Application of aerogeophysical data for gold exploration: implications for Central Lapland Greenstone Belt. Gold in the Central Lapland Greenstone Belt, Finland. Geological Survey of Finland, Special Paper. 44, 171-192.
- [12] Akbari, Z., Rasa, I., Mohajjel, M., Adabi, M.H., & Yarmohammadi, A.M. (2015). Hydrothermal Alteration Identification of Ahangan Deposit, West of Iran Using ASTER Spectral Analysis. *International Geoinformatics Research and Development Journal*. 6, 1.
- [13] Aliyari, F., Rastad, E., & Mohajjel, M. (2012). Gold Deposits in the Sanandaj-Sirjan Zone: Orogenic Gold Deposits or Intrusion - Related Gold Systems? *Resource Geology*, 62(3), pp.296-315.
- [14] Aliyari, F., Rastad, E., Goldfarb, R.J., & Sharif, J.A. (2014). Geochemistry of hydrothermal alteration at the Qolqoleh gold deposit, northern Sanandaj-Sirjan metamorphic belt, northwestern Iran: Vectors to high-grade ore bodies. *Journal of geochemical exploration*. 140, 111-125.
- [15] Almasi, A., Yousefi, M., & Carranza, E.J.M. (2017). Prospectivity analysis of orogenic gold deposits in Saqez-Sardasht Goldfield, Zagros Orogen, Iran. *Ore Geology Reviews*. 91, 1066-1080.
- [16] Azad, M.R., Koneshloo, M., Rouhani, A.K., & Aghajani, H. (2016). Comparison of Factorial Kriging Analysis Method and Upward Continuation Filter to Recognize Subsurface Structures—A Case Study: Gravity Data from a Hydrocarbon Field in the Southeast Sedimentary Basins of the East Vietnam Sea. *Acta Geophysica*. 64(2), 398-416.
- [17] Azizi, H., Tarverdi, M.A., & Akbarpour, A. (2010). Extraction of hydrothermal alterations from ASTER SWIR data from east Zanjan, northern Iran. *Advances in Space Research*. 46(1), 99-109.
- [18] Bahiru, E.A., & Woldai, T. (2016). Integrated geological mapping approach and gold mineralization in Buhweju area, Uganda. *Ore Geology Reviews*. 72, 777-793.
- [19] Barak, S., Bahroudi, A., Jozanikohan, G., & Aslani, S. (2016). Geochemical Anomaly Separation by Using the Soil Samples of Eastern Neysian, Isfahan Province. *Geochemistry*. 5(1), 55-71.
- [20] Barak, S., Bahrodi, A., & Jozanikohan, G. (2018). The use of fuzzy inference system in the integration, *iranian journal of mining engineering* 13(38), 97-112.
- [21] Barak, S., Abedi, M., & Bahroudi, A. (2020). A knowledge-guided fuzzy inference approach for integrating geophysics, geochemistry, and geology data in a deposit-scale porphyry copper targeting, Saveh, Iran. *Bollettino di Geofisica Teorica ed Applicata*, 61(2).
- [22] Barak, S., Imamalipour, A., Abedi, M., Bahroudi, A., & Khalifani, F. M. (2021). Comprehensive modeling of mineral potential mapping by integration of multiset geosciences data. *Geochemistry*, 81(4), 125824.
- [23] Carranza, E.J.M., & Laborte, A.G. (2015). Data-driven predictive mapping of gold prospectivity, Baguio district, Philippines: Application of Random Forests algorithm. *Ore Geology Reviews*. 7, 777-787.
- [24] Carranza, E.J.M., Sadeghi, M., & Billay, A. (2015). Predictive mapping of prospectivity for orogenic gold, Giyani greenstone belt (South Africa). *Ore Geology Reviews*. 71, 703-718.
- [25] Cooper, G.R.J., & Cowan, D.R. (2006). Enhancing potential field data using filters based on the local phase. *Computers &*

- Geosciences. 32(10), 1585-1591.
- [26] Cooper, G.R., & Cowan, D.R. (2008). Edge enhancement of potential-field data using normalized statistics. *Geophysics*. 73(3), H1-H4.
- [27] Elkhateeb, S.O., & Abdellatif, M.A.G. (2018). Delineation potential gold mineralization zones in a part of central Eastern Desert, Egypt using Airborne Magnetic and Radiometric data. *NRIAG Journal of Astronomy and Geophysics*.
- [28] Fan, M., Xiao, K., Sun, L., & Xu, Y. (2023). Metallogenic prediction based on geological-model driven and data-driven multisource information fusion: A case study of gold deposits in Xiongershan area, Henan Province, China. *Ore Geology Reviews*, p.105390.
- [29] Fatehi, M., & Asadi, H.H. (2017). Application of semi-supervised fuzzy c-means method in clustering multivariate geochemical data, a case study from the Dalli Cu-Au porphyry deposit in central Iran. *Ore Geology Reviews*. 81, 245-255.
- [30] Gabr, S., Ghulam, A., & Kusky, T. (2010). Detecting areas of high-potential gold mineralization using ASTER data. *Ore Geology Reviews*. 38(1-2), 59-69.
- [31] Gabr, S.S., Diab, H., Fattah, T.A.A., Sadek, M.F., Khalil, K.I., & Youssef, M.A. (2022). Aeromagnetic and Landsat-8 data interpretation for structural and hydrothermal alteration mapping along the Central and Southern Eastern Desert boundary, Egypt. *The Egyptian Journal of Remote Sensing and Space Science*, 25(1), pp.11-20.
- [32] Gahlan, H.A., Azer, M.K., Asimow, P.D., & Al-Kahtany, K.M. (2022). Formation of gold-bearing listvenite in the mantle section of the Neoproterozoic Bir Umq ophiolite, Western Arabian Shield, Saudi Arabia. *Journal of African Earth Sciences*, 190, p.104517.
- [33] Ghasemi, A., & Talbot, C.J. (2006). A new tectonic scenario for the Sanandaj-Sirjan Zone (Iran). *Journal of Asian Earth Sciences*. 26(6), 683-693.
- [34] Ghasemzadeh, S., Maghsoudi, A., Yousefi, M., & Mihalasky, M.J. (2019). Stream sediment geochemical data analysis for district-scale mineral exploration targeting: Measuring the performance of the spatial U-statistic and CA fractal modeling. *Ore Geology Reviews*, 113, 103115.
- [35] Ghasemzadeh, S., Maghsoudi, A., Yousefi, M., & Mihalasky, M.J. (2022). Information value-based geochemical anomaly modeling: A statistical index to generate enhanced geochemical signatures for mineral exploration targeting. *Applied Geochemistry*, 136, 105177.
- [36] Ghiasi, S.M., Hosseini, S.H., Afshar, A., & Abedi, M. (2023). A novel magnetic interpretational perspective on charmaleh iron deposit through improved edge detection techniques and 3D inversion approaches. *Natural Resources Research*, 32(1), pp.147-170.
- [37] Glennie, K.W. (2000). Cretaceous tectonic evolution of Arabia's eastern plate margin: a tale of two oceans.
- [38] Goldfarb, R.J., Groves, D.I., & Gardoll, S. (2001). Orogenic gold and geologic time: a global synthesis. *Ore geology reviews*. 18(1-2), 1-75.
- [39] Goldfarb, R.J., & Groves, D.I. (2015). Orogenic gold: Common or evolving fluid and metal sources through time. *Lithos*, 233, pp.2-26.
- [40] Hassanpour, S., & Afzal, P. (2013). Application of concentration-number (C-N) multifractal modeling for geochemical anomaly separation in Haftcheshmeh porphyry system, NW Iran. *Arabian Journal of Geosciences*. 6(3), 957-970.
- [41] Hosseini, S.A., Khah, N.K.F., Kianoush, P., Afzal, P., Ebrahimabadi, A., & Shirinabadi, R. (2023). Integration of Fractal modeling and Correspondence Analysis Reconnaissance for Geochemically High-Potential Promising Areas, NE Iran. *Results in Geochemistry*, p.100026.
- [42] Imamalipour, A., & Barak, S. (2019). Geochemistry and tectonic setting of the volcanic host rocks of VMS mineralisation in the Qezil Dash area, NW Iran: implications for prospecting of Cyprus-type VMS deposits in the Khoy ophiolite. *Geological Quarterly*, 63(3).
- [43] Imamalipour, A., Barak, S., & Khalifani, F.M. (2020). Quantifying mass changes during hydrothermal alteration in listwaenite-type mercury mineralization, Tavreh area, northwestern Iran. *Geochemistry: Exploration, Environment, Analysis*, 20(4), 425-439.
- [44] Kruse, F.A., Lefkoff, A.B., Boardman, J.W., Heidebrecht, K.B., Shapiro, A.T., Barloon, P.J., & Goetz, A.F.H. (1993). The spectral image processing system (SIPS) interactive visualization and analysis of imaging spectrometer data. *Remote sensing of environment*. 44(2-3), 145-163.
- [45] Magalhães, L.A., & Souza Filho, C.R. (2012). Targeting of gold deposits in Amazonian exploration frontiers using knowledge-and data-driven spatial modeling of geophysical, geochemical, and geological data. *Surveys in Geophysics*. 33(2), 211-241.
- [46] Mami Khalifani, F., Bahroudi, A., Mohebi, A., Aslani, S., Jozanikohan, G., & Barak, S. (2016). Geochemical anomaly separation using the multivariate statistical methods in Saqqez Region, 4th International Mine and Mining Industries Congress & 6th Iranian Mining Engineering Conference. Teharn, Iran.
- [47] Mami Khalifani, F., Bahroudi, A., Barak, S., & Jozani, G. (2018a). Geochemical exploration of orogenic gold deposit using Concentration-number (C-N) fractal and probability-number (P.N) methods in the NW of the Sanandaj-Sirjan Zone", The 10th Iranian Economic Geology Conference, ISC, University of Isfahan (UI).
- [48] Mami Khalifani, F., Bahroudi, A., Barak, S., Abedi, M., & Mohammadpour, M. (2018b). Integrated exploration of orogenic gold mineralization in the northwest of Iran, Saqez area, integrated exploration of orogenic gold mineralization in the northwest of Iran, Saqez area, The 10th Iranian Economic Geology Conference, Isfahan, Iran.
- [49] Mami Khalifani, F., Bahroudi, A., Abedi, M., & Mohammadpour, M. (2019). Integrated exploration of orogenic gold mineralization in the northwest of Iran, Saqez area, integrated exploration of orogenic gold mineralization in the northwest of Iran, Saqez area, The 10th Iranian Economic Geology Conference, Isfahan, Iran.
- [50] Mavrantza, O., & Argialas, D.P. (2003). Implementation and evaluation of spatial filtering and edge detection techniques for lineament mapping: case study-Alevrada, Central Greece. In *Remote Sensing for Environmental Monitoring, GIS Applications, and Geology*. 4886, 417-429. International Society for Optics and Photonics.
- [51] Mekkawi, M.M., Abd-El-Nabi, S.H., Farag, K.S., & Abd Elhamid, M.Y. (2022). Geothermal resources prospecting using magnetotelluric and magnetic methods at Al Ain

- AlSukhuna-Al Galala Albahariya area, Gulf of Suez, Egypt. *Journal of African Earth Sciences*, 190, p.104522.
- [52] Mohebi, A., Mirnejad, H., Lentz, D., Behzadi, M., Dolati, A., Kani, A., & Taghizadeh, H. (2015). Controls on porphyry Cu mineralization around Hanza Mountain, south-east of Iran: an analysis of structural evolution from remote sensing, geophysical, geochemical and geological data. *Ore Geology Reviews*. 69, 187-198.
- [53] Mohamed Taha, A.M., Xi, Y., He, Q., Hu, A., Wang, S., & Liu, X. (2022). Investigating the Capabilities of Various Multispectral Remote Sensors Data to Map Mineral Prospectivity Based on Random Forest Predictive Model: A Case Study for Gold Deposits in Hamissana Area, NE Sudan. *Minerals*, 13(1), p.49.
- [54] Mokhtari, A.R., Cohen, D.R., & Gatehouse, S.G. (2009). Geochemical effects of deeply buried Cu–Au mineralization on transported regolith in an arid terrain. *Geochemistry: Exploration, Environment and Analysis*. 9, 227–236.
- [55] Müller, D., Kwan, K., & Groves, D.I. (2022). Integrated geophysical signatures and structural geometry of the Kabinakagami Lake greenstone belt, Superior Province, Ontario, Canada: Exploration implications for concealed Archean orogenic gold deposits. *Journal of Applied Geophysics*, 199, p.104613.
- [56] Nigm, A.A., Youssef, M.A., & Abdelwahab, F.M. (2018). Airborn gamma-ray spectrometric data as guide for probable hydrocarbon accumulations at Al-Laqtah area, Central Eastern Desert of Egypt. *Applied Radiation and Isotopes*. 132, 38-46.
- [57] Núñez-Demarco, P., Bonilla, A., Sánchez-Bettucci, L., & Prezzi, C. (2023). Potential-field filters for gravity and magnetic interpretation: a review. *Surveys in Geophysics*, 44(3), pp.603-664.
- [58] Nykänen, V., Groves, D.I., Ojala, V.J., & Gardoll, S.J. (2008). Combined conceptual/empirical prospectivity mapping for orogenic gold in the northern Fennoscandian Shield, Finland. *Australian Journal of Earth Science*. 55(1), 39-59.
- [59] Pour, A.B., & Hashim, M. (2015a). Structural mapping using PALSAR data in the Central Gold Belt, Peninsular Malaysia. *Ore Geology Reviews*. 64, 13-22.
- [60] Pour, A.B., & Hashim, M. (2015b). Hydrothermal alteration mapping from Landsat-8 data, Sar Cheshmeh copper mining district, south-eastern Islamic Republic of Iran. *Journal of Taibah University for Science*. 9(2), 155-166.
- [61] Prabakaran, S., & Subramani, T. (2016). Identification of hydrocarbon micro-seeps based on mineral alteration in a part of Cauvery Basin, South India using Hyperion Data.
- [62] Rahimi, H., Abedi, M., Yousefi, M., Bahroudi, A., & Elyasi, G.R. (2021). Supervised mineral exploration targeting and the challenges with the selection of deposit and non-deposit sites thereof. *Applied Geochemistry*, 128, 104940.
- [63] Rahmati, A., Afzal, P., Abrishamifar, S.A., & Sadeghi, B. (2015). Application of concentration–number and concentration–volume fractal models to delineate mineralized zones in the Sheytoor iron deposit, Central Iran. *Arabian Journal of Geosciences*. 8(5), 2953-2965.
- [64] Reeves, C. (2005). *Aeromagnetic surveys: principles, practice and interpretation* (Vol. 155). Geosoft.
- [65] Rezaie, M., Moradzadeh, A., Aghajani, H., & Nejati, A. (2016). Imaging Ojatabad iron ore using magnetic data.
- [66] Rezaie, M., Moradzadeh, A., & Kalateh, A.N. (2017). Fast 3D inversion of gravity data using solution space priorconditioned lanczos bidiagonalization. *Journal of Applied Geophysics*. 136, 42-50.
- [67] Sabzai, M., Eshraghi, S.A., & Roshan-Ravan, J. (1997). *Geological Map of Sirjan* (1: 100,000). Geological Survey of Iran.
- [68] Siemon, B., Ibs-von Seht, M., Steuer, A., Deus, N., & Wiederhold, H. (2020). Airborne electromagnetic, magnetic, and radiometric surveys at the German North Sea coast applied to groundwater and soil investigations. *Remote Sensing*, 12(10), p.1629.
- [69] Silva, A.M., Pires, A.C.B., Mccafferty, A., de Moraes, R.A.V., & Xia, H. (2003). Application of airborne geophysical data to mineral exploration in the uneven exposed terrains of the Rio Das Velhas greenstone belt. *Brazilian Journal of Geology*. 33(2), 17-28.
- [70] Stampfli, G.M., & Borel, G.D. (2002). A plate tectonic model for the Paleozoic and Mesozoic constrained by dynamic plate boundaries and restored synthetic oceanic isochrons. *Earth and Planetary Science Letters*. 19(1), 17-33.
- [71] Sukumar, M. (2017). Performance evaluation of lineament extraction methods in ASTER satellite images. *International Journal of Oceans and Oceanography*. 11(2), 249-263.
- [72] Sun, Y., Tian, S., & Di, B. (2017). Extracting mineral alteration information using WorldView-3 data. *Geoscience Frontiers*. 8(5), 1051-1062.
- [73] Weyermann, J., Schläpfer, D., Hueni, A., Kneubühler, M., & Schaepman, M. (2009). Spectral angle mapper (SAM) for anisotropy class indexing in imaging spectrometry data. In *Imaging Spectrometry 7457-74570B*. International Society for Optics and Photonics.
- [74] Yilmaz, H. (2003a). Geochemical exploration for gold in western Turkey: success and failure. *Journal of Geochemical Exploration*. 80, 117-135.
- [75] Yilmaz, H. (2003b). Exploration at the Kuscaiyiri Au (Cu) prospect and its implications for porphyry-related Au (Cu) mineralization in western Turkey. *Journal of Geochemical Exploration*. 77, 133–150.
- [76] Yilmaz, H., Sönmez, F.N., & Carranza, E.J.M. (2015). Discovery of Au–Ag mineralization by stream sediment and soil geochemical exploration in metamorphic terrain in western Turkey. *Journal of Geochemical Exploration*. 158, 55-73.
- [77] Yousefi, M., Carranza, E.J.M., & Kamkar-Rouhani. (2013). Weighted drainage catchment basin mapping of stream sediment geochemical anomalies for mineral potential mapping. *Journal of Geochemical Exploration*. 128, 88-96.
- [78] Yousefi, M., Kamkar-Rouhani, A., & Carranza, E.J.M. (2014). Application of staged factor analysis and logistic function to create a fuzzy stream sediment geochemical evidence layer for mineral prospectivity mapping. *Geochemistry: Exploration, Environmental, Analysis*. 14, 45-58.
- [79] Yousefi, M. (2017a). Recognition of an enhanced multi-element geochemical signature of porphyry copper deposits for vectoring into mineralized zones and delimiting exploration targets in Jiroft area, SE Iran. *Ore Geology Reviews*. 83, 200-214.
- [80] Yousefi, M. (2017b). Analysis of zoning pattern of geochemical indicators for targeting of Porphyry-Cu

- mineralization: A pixel-based mapping approach. *Natural Resources Research*. 26(4), 429-441.
- [81] Yousefi, M., & Hronsky, J.M. (2023). Translation of the function of hydrothermal mineralization-related focused fluid flux into a mappable exploration criterion for mineral exploration targeting. *Applied Geochemistry*, 105561.
- [82] Zadeh, M.H., Tangestani, M.H., Roldan, F.V., & Yusta, I. (2014a). Spectral characteristics of minerals in alteration zones associated with porphyry copper deposits in the middle part of Kerman copper belt, SE Iran. *Ore Geology Reviews*. 62, 191-198.
- [83] Zadeh, M.H., Tangestani, M.H., Roldan, F.V., & Yusta, I. (2014b). Sub-pixel mineral mapping of a porphyry copper belt using EO-1 Hyperion data. *Advances in Space Research*. 53(3), 440-451.
- [84] Zuo, R. (2011). Identifying geochemical anomalies associated with Cu and Pb–Zn skarn mineralization using principal component analysis and spectrum–area fractal modeling in the Gangdese Belt, Tibet (China). *Journal of Geochemical Exploration*. 111, (1-2), 13-22.